

Mutation of Glu-166 Blocks the Substrate-Induced Dimerization of SARS Coronavirus Main Protease

Shu-Chun Cheng, Gu-Gang Chang, and Chi-Yuan Chou*

Department of Life Sciences and Institute of Genome Sciences, National Yang-Ming University, Taipei, Taiwan, Republic of China

ABSTRACT The maturation of SARS coronavirus involves the autocleavage of polyproteins 1a and 1ab by the main protease (Mpro) and a papain-like protease; these represent attractive targets for the development of anti-SARS drugs. The functional unit of Mpro is a homodimer, and each subunit has a His-41···Cys-145 catalytic dyad. Current thinking in this area is that Mpro dimerization is essential for catalysis, although the influence of the substrate binding on the dimer formation has never been explored. Here, we delineate the contributions of the peptide substrate to Mpro dimerization. Enzyme kinetic assays indicate that the monomeric mutant R298A/L exhibits lower activity but in a cooperative manner. Analytical ultracentrifugation analyses indicate that in the presence of substrates, the major species of R298A/L shows a significant size shift toward the dimeric form and the monomer-dimer dissociation constant of R298A/L decreases by 12- to 17-fold, approaching that for wild-type. Furthermore, this substrate-induced dimerization was found to be reversible after substrates were removed. Based on the crystal structures, a key residue, Glu-166, which is responsible for recognizing the Gln-P1 of the substrate and binding to Ser-1 of another protomer, will interact with Asn-142 and block the S1 subsite entrance in the monomer. Our studies indicate that mutation of Glu-166 in the R298A mutant indeed blocks the substrate-induced dimerization. This demonstrates that Glu-166 plays a pivotal role in connecting the substrate binding site with the dimer interface. We conclude that protein-ligand and protein-protein interactions are closely correlated in Mpro.

INTRODUCTION

Severe acute respiratory syndrome (SARS) is an emerging infectious disease of this century and is caused by a novel coronavirus (CoV) termed SARS-CoV (1). During the outbreak in 2003, this virus infected >8000 people and the fatality rate in humans was as high as 15% (World Health Organization). In 2004 and 2005, the discovery of two more species of CoV that infect humans, NL-63 and HCoV-HKU1, confirm the high mutating rate and genetic recombination within Coronaviridae (2,3). The fact that the virus is easily transmitted between humans makes the re-emergence of SARS and other human CoVs a distinct possibility and has resulted in an urgent need to understand these viruses and their coding proteins.

SARS-CoV main protease (Mpro) cleaves the virion polyproteins (pp1a and 1b) at 11 sites that contain the canonical L-Q-↓-(A/S) sequence (4,5). Mpro was the first of the SARS-CoV proteins to have its three-dimensional structure solved by crystallography (6). Recently, structures of other CoV Mpros such as TGEV, IBV, and HCoV-HKU1 have also been solved (7–9). Although the overall sequence identity of these Mpros is only 40–50%, the three-dimensional structures, especially the regions of dimer interface, catalytic dyad, and substrate binding site, are highly conserved (10). Therefore, the design of broad-spectrum inhibitors of Mpro appears to be feasible for drug development (11).

Mpro is a homodimer in which the two subunits are arranged perpendicular to each other. Each protomer comprises three distinct structural domains. The first two domains (residues 8–101 for domain I and residues 102–184 for domain II) have an antiparallel β -barrel structure, which forms a folding scaffold similar to other viral chymotrypsinlike proteases (7,12,13). Each subunit has its own substrate binding site consisting of a His-41···Cys-145 catalytic dyad located at the interface between domains I and II (Fig. 1). An oxyanion hole is formed by the main-chain amides of Gly-143, Ser-144, and Cys-145 (6). Interestingly, Mpro contains an extra domain (III), which consists of five α -helices (residues 201–306), and this is a specific feature of CoV Mpro (6–9).

The catalytic N-terminal domain and C-terminal domain III can fold independently. The N-terminal domain is a monomer that is able to fold correctly but is catalytically inactive (14). The extra domain III increases the structural stability of the catalytic domain by increasing the folding rate. Furthermore, domain III is involved in the dimerization of Mpro, which has important functional implications for this enzyme (15). The side chain of Arg-4 at the N-finger (residues 1–7) of protomer A fits into a pocket of protomer B and forms a salt bridge with Glu-290; this constitutes one of the major interactions between the two subunits (16). Our previous studies have shown that N-terminal truncation of the whole N-finger results in almost complete loss of enzymatic activity (17). Critical N-terminal amino acid residues up to Arg-4 and C-terminal residues up to Gln-299 have been identified as involved in dimerization and thus in generating the correct conformation of the active

Submitted October 20, 2009, and accepted for publication December 7, 2009.

*Correspondence: cychou@ym.edu.tw

Editor: Patrick Loria.

© 2010 by the Biophysical Society
0006-3495/10/04/1327/10 \$2.00

doi: 10.1016/j.bpj.2009.12.4272

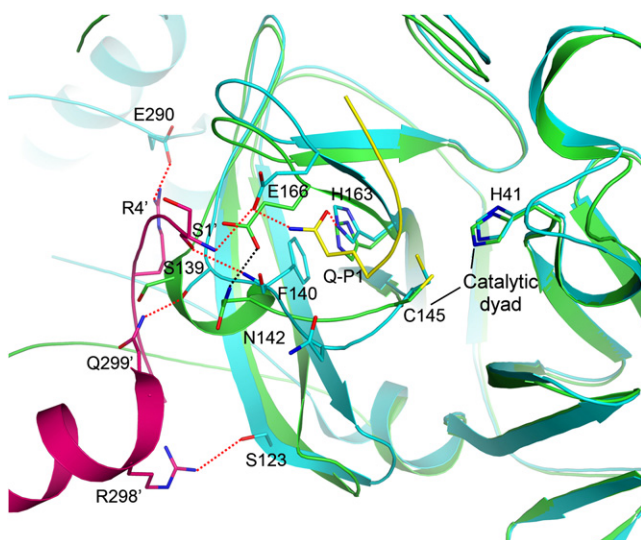


FIGURE 1 Active center of the SARS-CoV Mpro. The interactions between the P1 substrate-binding subsite from chain A (cyan) and the N-finger and domain III from chain B (magenta) of SARS-CoV Mpro (PDB code 1UK4) are shown. The substrate analog and the side chain of the Gln-P1 residue are yellow. The R298A monomeric structure (green) (PDB code 2QCY) is superimposed on the wild-type chain A. The dashed lines indicate hydrogen bonds for 1UK4 (red) and 2QCY (black). This figure was produced using PyMOL (35).

site (17,18). In addition, the interactions between the two helices A' (residues 11–15) and the S1 substrate-binding subsite, consisting of Phe-140, His-163, Met-165, Glu-166, and His-172, are also regarded as major components of the dimer interface (19,20).

Compared with functional dimeric Mpro, the crystal structures of monomeric Mpro (G11A, S139A, and R298A) have provided direct structural evidence for the catalytic incompetence of the dissociated monomer (19–21). In the monomer mutants, the oxyanion loop (Ser-139 to Leu-141) is converted into a short 3_{10} -helix and completely collapses inward, as exemplified by the large movement of Asn-142 and Leu-141. The slipped Asn-142 interacts with the side chain of Glu-166 and blocks entry to the S1 subsite; this results in enzyme inactivation (Fig. 1) (20). All experimental results have indicated that the dimerization of Mpro is essential for catalysis. Here, we provide what we believe is a novel approach that shows the influence of substrate binding on Mpro dimerization. Various biochemical and biophysical techniques are used to demonstrate the importance of substrate-induced dimerization to the catalytic mechanism of Mpro. By mutagenesis studies, a key residue, Glu-166, is found to play a connecting role between the substrate binding site and the dimer interface. We believe that this study will help deepen our understanding of the correlation between protein-ligand and protein-protein interactions in Mpro. Such an understanding will aid the development of new approaches to control SARS-CoV and other CoVs.

MATERIALS AND METHODS

Preparation of recombinant SARS-CoV Mpro

The construction of the expression plasmids for wild-type Mpro, R298A, R298L, and R298A/Q299A mutants have been described previously (16,18). For the site-directed mutagenesis (22) of E166A, the forward primer was 5'-tgctatgcatcatatggcgctccaacaggagtagac and the reverse primer was 5'-gtgtactcctgttgaagcgccatgatgatcatag. The polymerase chain reaction products were then treated with *DpnI* and transformed into *Escherichia coli* cells and checked by autosequencing. Next, the plasmids were transformed into *E. coli* strain BL21 (DE3) cells. The cells were grown in Luria-Bertani medium with 50 $\mu\text{g/ml}$ Kanamycin at 37°C. After 3 h incubation, the cells were induced overnight by 0.4 mM isopropyl-1-thio- β -D-galactoside at 20°C. For purification, all operations were performed at 4°C. The cells were centrifuged at $6000 \times g$ for 10 min. The supernatant was removed and the pellets were resuspended in the lysis buffer (20 mM Tris-Cl, 250 mM NaCl, 2 mM β -mercaptoethanol (β -ME), and 0.2% Triton X-100, pH 8.5). The cells were then sonicated using sixty 10-s bursts at 300 W with a 10-s cooling period between each burst. The cell debris was removed by centrifugation ($10,000 \times g$ for 25 min). Lysis buffer-equilibrated Ni-NTA slurry (Qiagen, Hilden, Germany) (1 ml) was then added to the soluble lysate, followed by gentle mixing for 1 h. The mixture was then loaded into a column and washed with the washing buffer (20 mM Tris-Cl, 250 mM NaCl, 8 mM imidazole, and 2 mM β -ME, pH 8.5). Finally, the protease was eluted with elution buffer (20 mM Tris-Cl, 30 mM NaCl, 150 mM imidazole, and 2 mM β -ME, pH 8.5).

The purified enzyme was concentrated and the buffer replaced using phosphate-buffered saline (20 mM sodium phosphate buffer, 150 mM NaCl, and 2 mM β -ME, pH 7.6) and an Amicon Ultra-4 centrifugal filter with a mass cutoff at 10 kDa (Millipore, Bedford, MA). Samples from this purification step were subjected to SDS-PAGE to check for homogeneity (>95% purity). Typical yields of the enzyme after purification were 5–10 mg from 1 liter of *E. coli* culture medium.

Enzyme kinetic assay

The enzymatic activity of Mpro was measured by a colorimetry-based peptide cleavage assay involving the 6-mer peptide substrate TSAVLQ-para-nitroanilide (TQ6-pNA) (purity 95–99% by high-performance liquid chromatography; GL Biochem, Shanghai, China) (23). This substrate is cleaved at the Gln-pNA bond to release free pNA, which turns the solution color to yellow. The increase in absorbance at 405 nm was continuously monitored using a Jasco V-550 UV/VIS spectrophotometer (Tokyo, Japan). The amount of pNA released from the proteolysis can be calculated with a standard curve generated by analytical-grade pNA, which is consistent with the absorbance reported in the literature ($A_{405 \text{ nm}} = 9.8$ at 1 mM) (24).

The protease activity assay was performed in 10 mM phosphate (pH 7.6) at 30°C. The substrate stock solution was 1 mM and the working concentrations were 5–950 μM . In the substrate titration assay, the concentrations of Mpro, E166A, and R298A/L mutants were 1, 5.7, and 2.6 μM , respectively. The steady-state enzyme kinetic parameters were obtained by fitting the initial velocity (v_0) data to the Michaelis-Menten equation (Eq. 1):

$$v_0 = \frac{k_{\text{cat}}[E][S]}{K_m + [S]}, \quad (1)$$

where k_{cat} is the catalytic constant, $[E]$ is the enzyme concentration, $[S]$ is the substrate concentration, and K_m is the Michaelis constant of the substrate. The program SigmaPlot (Systat Software, Richmond, CA) was used for the data analysis.

For the cooperativity effect, the kinetic parameters were obtained by fitting the initial velocities to the Hill equation (Eq. 2):

$$v_0 = \frac{k_{\text{cat}}[E][S]^h}{K' + [S]^h}, \quad (2)$$

where K' is a constant that relates to the dissociation constant and h is the Hill constant.

The dependence of the proteolytic activity on enzyme concentration was investigated for the wild-type Mpro and R298A/L mutants, at a substrate concentration of 600 μ M TQ6-pNA. The initial velocity of the reaction at various concentrations of each enzyme was determined and fitted to the nonlinear dependence equation (Eq. 3):

$$v_0 = k_{\text{cat}} \left(K_d + 4[E] - \sqrt{K_d^2 + 8K_d[E]} \right) / 8, \quad (3)$$

where K_d is the monomer-dimer dissociation constant.

Analytical ultracentrifugation analysis

The analytical ultracentrifugation (AUC) experiments were performed on an XL-A analytical ultracentrifuge (Beckman, Fullerton, CA) with an An-50 Ti rotor (17). The sedimentation velocity (SV) experiments were performed in a double-sector *epon* charcoal-filled centerpiece at 20°C with a rotor speed of 42,000 rpm. The sample (330 μ l) and reference (370 μ l) solutions with or without different concentrations of TQ6-pNA substrate were loaded into the centerpiece. We found that the TQ6-pNA was cleaved and free pNA was released in the process of centrifugation (detected by absorbance at 405 nm). The absorbance spectrum of free pNA interfered with protein absorbance at 280 nm. Therefore, absorbance at 250 nm was chosen to detect the protein, which was monitored in a continuous mode with a time interval of 480 s and a step size of 0.003 cm. Three different protein concentrations (from 1.4 to 57.2 μ M) were used to estimate the dynamic monomer-dimer content. Multiple scans at different time intervals were then fitted to a continuous $c(s)$ distribution model using the SEDFIT program (25,26). The partial specific volume of Mpro, the solvent density, and the viscosity were calculated by SEDNTERP (<http://www.jphilo.mailway.com/download.htm>) (cited Oct. 20, 2009).

The sedimentation equilibrium (SE) experiments were performed in a six-channel centerpiece. Three different samples (0.10–0.12 ml) were loaded into the sample channels and 0.11–13 ml buffers were loaded into the reference channels. The cells were then loaded into the rotor and run at multispeeding (8000, 12,000, and 15,000 rpm), each for 12 h at 20°C. Ten scans of absorbance at 250 nm at time intervals of 10 min were measured for every rotor speed to check the status of SE. In our studies, all Mpro and its mutants were able to achieve equilibrium state after 12 h. The SV results at three protein concentrations and the multispeed SE data were then globally analyzed using a monomer-dimer equilibrium model by the SEDPHAT program (27), which gives a precise measurement for K_d and the dissociation rate constant (k_{off}) (18,28,29).

Analytical size-exclusive chromatography

Size-exclusive chromatographic experiments were performed using a GE Healthcare ÄKTA purifier system (Pittsburgh, PA) with a Superose 12 (10/300) column preequilibrated with phosphate-buffered saline (pH 7.6). Mpro and its mutants without or with 600 μ M of substrate preincubation for 20 min were injected into the column separately. The elution was carried out at a flow rate of 0.5 ml/min and the absorbance at 280 nm was monitored continuously.

Isothermal titration calorimetry

The isothermal titration calorimetry (ITC) protocol followed was that of Sondermann et al. (30) with some modifications. Apparent dissociation constants and stoichiometry of the enzyme-ligand interactions were measured by a thermal activity monitor (2277, TA instruments, New Castle, DE). Calorimetric titrations of the peptide substrate TQ6-pNA (1 mM in a 250- μ l syringe) and Mpro (5.7 μ M for wild-type and 28.6 μ M for mutants in a 4-ml ampoule) were carried out at 25°C in 10 mM phosphate buffer (pH 7.6). The peptides were titrated into the enzyme in 10- μ l aliquots per injection with a time interval of 20 min. A control experiment in the absence

of enzyme was performed in parallel to correct for the dilution of heat. The data were then analyzed by integrating the heat effects normalized to the amount of injected proteins using curve fitting based on a 1:1 binding model. This involved the use of Digitam software (TA instruments).

RESULTS AND DISCUSSION

Cooperative effect of initial velocity curves of R298A and R298L mutants

To measure the activity of Mpro and its mutants, we used the 6-mer substrate peptide (TSAVLQ) attached to a pNA group (23). This peptide is specifically cleaved by SARS-CoV Mpro at the designated site (Gln-pNA) to release free pNA, which results in an increased absorbance at 405 nm. Besides wild-type Mpro as a dimeric target, two single mutants, R298A and R298L, and one double mutant, R298A/Q299A, were chosen as the monomeric targets. According to previous studies (19), mutation of R298 or Q299 will induce dimer dissociation and result in an ~10-fold decrease in proteolytic activity (18). When R298 and Q299 are both mutated, the enzyme activity decreases by 100-fold. Other studies also suggest that the monomeric Mpro by other mutations shows very low or no proteolytic activity (16–21,31). Indeed, in this study, we were not able to detect any enzyme activity associated with the R298A/Q299A double mutant. However, for the single mutants, R298A or R298L, the initial velocity pattern at various substrate concentrations displayed a sigmoid curve (Fig. 2, B and C). The dimeric Mpro, on the other hand, exhibited a classical saturation curve (Fig. 2 A). These results were then fitted to the Michaelis-Menten or Hill equations to evaluate the kinetic parameters. The best-fit results are shown in Table 1. The K_m (223 μ M) and k_{cat} (0.63 s⁻¹) of wild-type Mpro with TQ6-pNA substrate are close to observations from other laboratories (23,32). After fitting to the Hill equation, the k_{cat} of R298A was sixfold lower than that of the wild-type enzyme. In contrast, R298L showed a k_{cat} close to that of the wild-type enzyme. The Hill constants of R298A and R298L were 2.0 and 1.8, respectively. This nonunity number suggested that there is a strong positive cooperativity among the Mpro protomers. However, since the cooperativity phenomenon is not compatible with a monomeric form, we sought other evidence to examine the possibility of dimeric Mpro formation during the catalytic process.

Nonlinear dependence of initial velocity on protease concentration

The dependence of the initial velocity on protease concentration was analyzed (Fig. 2, D–F). If the monomeric Mpro has an activity identical to that of the dimeric one, a linear pattern should be obtained (28). However, a nonlinear positive correlation was observed for the wild-type and R298A/L monomeric mutants. After fitting to the nonlinear dependence equation (Eq. 3), the k_{cat} (Table 1) and K_d for the monomer-dimer equilibrium (Table 2) were calculated.

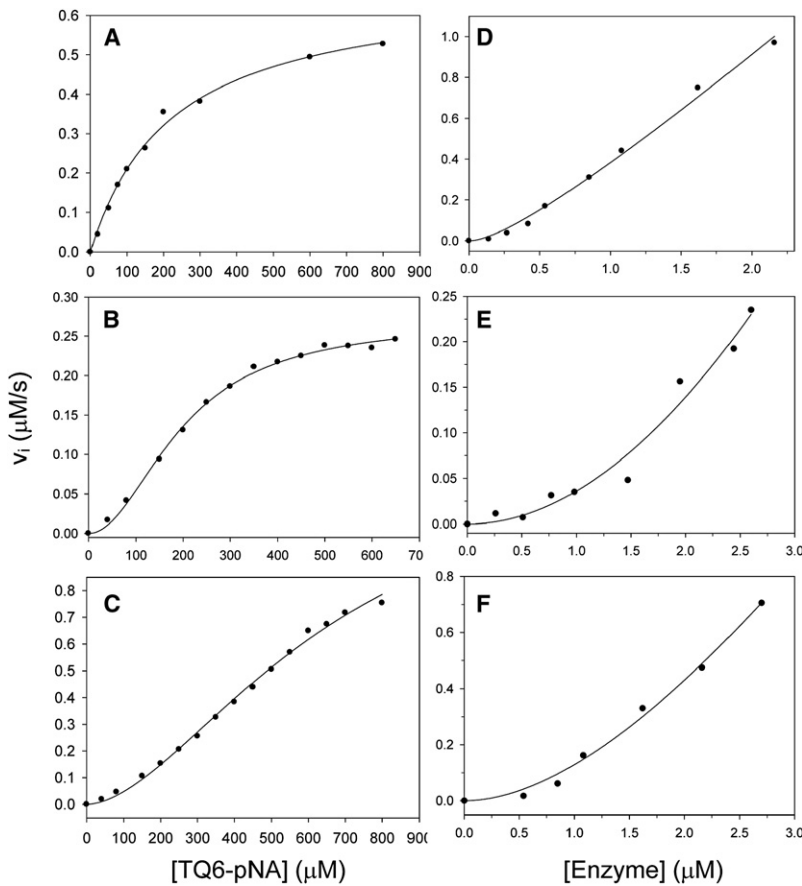


FIGURE 2 Initial velocity patterns of Mpro (A–C) and dependence of the initial velocity of Mpro on enzyme concentration (D–F). (A–C) Plots of the velocity difference at various substrate concentrations for wild-type, R298A, and R298L mutants, respectively. The lines represent results fitted according to the Michaelis-Menten equation (Eq. 1) for wild-type and the Hill equation (Eq. 2) for mutants. The kinetic parameters are shown in Table 1. (D–F) Difference in velocity at various enzyme concentrations for wild-type, R298A, and R298L mutants, respectively. The concentration of substrate was $600 \mu\text{M}$. The line represents the best fit to the nonlinear dependence equation (Eq. 3).

The k_{cat} for wild-type and the mutants did not show any significant difference, whereas the K_d values for R298A/L were increased from 14- to 17-fold, indicating that the R298A/L mutants are more easily dissociated. The nonlinear dependence detected here suggests that proteolytic activity is actually related to the dimer content, which in turn is influenced by the protein concentration. Based on this, we next

TABLE 1 Kinetic parameters of Mpro and its mutants

Protein	K_m (μM)*	k_{cat} (s^{-1})*	k_{cat}/K_m ($\text{s}^{-1} \text{M}^{-1}$)	k_{cat} (s^{-1}) by nonlinear fitting [†]
Wild-type	222.6 ± 19.0	0.63 ± 0.02	2830 ± 303	1.4 ± 0.2
E166A	353.4 ± 48.0	0.31 ± 0.01	877 ± 132	ND [‡]
	K' ($10^4 \mu\text{M}$)	k_{cat} (s^{-1})	h	
R298A	3.9 ± 2.3	0.10 ± 0.004	2.0 ± 0.1	0.7 ± 0.4
R298L	9.5 ± 6.2	0.48 ± 0.06	1.8 ± 0.1	2.3 ± 0.9

*Data of wild-type Mpro and E166A mutant were fitted to the Michaelis-Menten equation (Eq. 1) and the R_{sqr} values were 0.994 and 0.987, respectively. Those of mutants were fitted to the Hill equation (Eq. 2), and the R_{sqr} values were 0.998 and 0.996, respectively. All the assays were repeated several times to ensure reproducibility.

[†]Catalytic constant was calculated by the nonlinear dependence equation (Eq. 3). The best-fitting R_{sqr} values for wild-type, R298A, and R298L were 0.995, 0.99 and 0.993, respectively.

[‡]Not determined.

performed AUC experiments on Mpro with or without the presence of peptide substrates to evaluate the quaternary structural changes during the catalytic process.

Dimeric R298A and R298L mutants in the presence of peptide substrates can be detected by AUC

Interestingly, wild-type Mpro and the R298 mutants displayed different monomer-dimer equilibrium with or without substrates. A typical SV experiment of AUC is shown in Fig. 3 A. The cumulative spectra were analyzed using the continuous size distribution model (26), which shows the quaternary structure distribution and the sedimentation coefficients (S) (Fig. 3, B–E). Although wild-type Mpro maintained a stable dimeric form, the R298A/Q299A double mutant existed exclusively in monomeric form irrespective of the presence of high concentrations of substrate (Fig. 3, B and E). Here, we confirmed that the monomeric and dimeric Mpro sedimented at 2.9 and 4.1 S, respectively. These values are consistent with previous observations (16,18,21).

However, a different story was found for the R298 single mutants. In the presence of substrates, the R298A and R298L mutants showed a significant shifting of the major species (Fig. 3, C and D). At $600 \mu\text{M}$ TQ6-pNA, the major species

TABLE 2 Dissociation of Mpro and its mutants with and without substrates

Protein	Nonlinear fitting			AUC analysis	
	K_d (μM)*	No substrate		With 600 μM substrate	
		K_d (μM) [†]	k_{off} (s^{-1}) [†]	K_d (μM) [†]	k_{off} (s^{-1}) [†]
Wild-type	0.8 ± 0.4	2.0 ± 0.01	0.1 ± 0.007	1.7 ± 0.03	0.1 ± 0.002
R298A	11.4 ± 9.7	81.1 ± 3.3	0.1 ± 0.004	4.7 ± 0.1	0.08 ± 0.001
R298L	13.8 ± 8.7	30.8 ± 0.4	0.1 ± 0.001	2.6 ± 0.1	0.1 ± 0.003
R298A/Q299A	ND ^c	85.7 ± 3.1	0.1 ± 0.004	115.0 ± 4.4	0.05 ± 0.002
E166A	ND	3.7 ± 0.2	0.04 ± 0.001	0.4 ± 0.01	0.1 ± 0.002
E166A/R298A	ND	141.1 ± 12.7	0.1 ± 0.009	103.7 ± 8.3	0.06 ± 0.005

* K_d was calculated by nonlinear dependence equation (Eq. 3).

[†]Parameters were derived from a global fit of the SV and SE data to a monomer-dimer self-association model by SEDPHAT. The SE experiments for the assay were obtained at protein concentrations of 5.7–28.6 μM , whereas SV experiments were at 1.4–57.2 μM .

of R298A/L shifted from 2.9 S to 3.8–3.9 S. The distribution now became a broad peak between the monomer and dimer, but closer to the dimer. In a fast dissociated and associated system, a broad size distribution will appear between the monomer and dimer when the protein concentration is close to the K_d (27). Thus, SARS-CoV Mpro acts as a rapid monomer-dimer self-association equilibrium system. Furthermore, we also measured the size distribution of R298A at various substrate concentrations. The results clearly indicated that the distance of major species shifting was related to the substrate dosage (Fig. 4 A). More substrates resulted in more of the dimer form and the major species became closer and closer to the dimer. The trend was a linear positive correlation (Fig. 4 B). Therefore, we conclude that the presence of substrate can induce a quaternary structural change in the R298A/L mutants. The system described in this article prevents any further monomer-dimer equilibrium analysis of the broad size distribution among the monomer and dimer species. We therefore performed the next set of experiments to further delineate the monomer-dimer equilibrium.

Monomer and dimer distribution of R298A/L mutants can be clearly delineated in deuterium water

To clearly separate the monomeric and dimeric signals, the speed of the protein self-association needs to be slowed down. To do this, we performed the same SV experiments in deuterium water (D_2O), which has a higher density (Fig. S1 A in the Supporting Material). All the buffer solutions and substrate stocks were prepared in D_2O to give the same ionic strengths. In the D_2O environment, the monomeric and dimeric Mpro sedimented at 1.9 and 2.6 S, respectively (Fig. S1, B and E). For the R298A mutant, there was a single monomeric form in the absence of substrate and a single dimeric form in the presence of substrate (Fig. S1 C). In addition, under the same conditions, both monomeric and dimeric forms of R298L could be observed (Fig. S1 D). This demonstrates that the high density of D_2O is able to slow down the exchange rate within the monomer-dimer equilibrium and clearly separate the signals from the two species.

We next analyzed the size distribution of the R298A mutant at various substrate concentrations in D_2O (Fig. S2 A). The results clearly indicate that the increase in dimeric form content is closely correlated with the substrate concentration (Fig. S2 B).

In summary, the measurements obtained by the SV experiments proved that the R298A/L mutants are able to associate into a dimeric form during the catalytic process. This substrate-induced dimerization is dose-dependent.

Dramatic decrease in dissociation constant in the presence of peptide substrate

To quantitatively characterize the monomer-dimer equilibrium of Mpro and its mutants, SV experiments were carried out at the three different enzyme concentrations with or without 600 μM TQ6-pNA. In addition, SE experiments were executed. The three SV and one SE datasets were then globally fitted to the monomer-dimer self-association model by SEDPHAT to estimate the K_d and k_{off} . The best-fit results are shown in Table 2. The k_{off} values for wild-type Mpro and its three mutants were all close to 0.1 s^{-1} , which indicates that the monomer-dimer exchange is instantaneous (27). The K_d values of wild-type Mpro without and with substrates were 2.0 and 1.7 μM , respectively, when those for the R298A/Q299A double mutant were 85 and 115 μM . Not surprisingly, the K_d of the R298A/L mutants was dramatically decreased, by 12- to 17-fold, in the presence of substrate, approaching the values for the wild-type (Table 2). The K_d rescued by substrates suggested that the R298A/L mutants display a protein association comparable to that of the wild-type in the presence of substrates. On the other hand, by nonlinear dependence fitting, the K_d of wild-type in the presence of substrates is 2.5-fold lower than in the absence of substrates (Table 2). The influence of substrates on the dimerization of wild-type is minor because of the stronger association between its protomers. In contrast, the R298A/Q299A double mutant lost two important ion pairs (Ser-123 (A)···Arg-298 (B) and Ser-139 (A)···Gln-299 (B)) in the dimer interface (18) and results in complete dissociation, even in the presence of substrates.

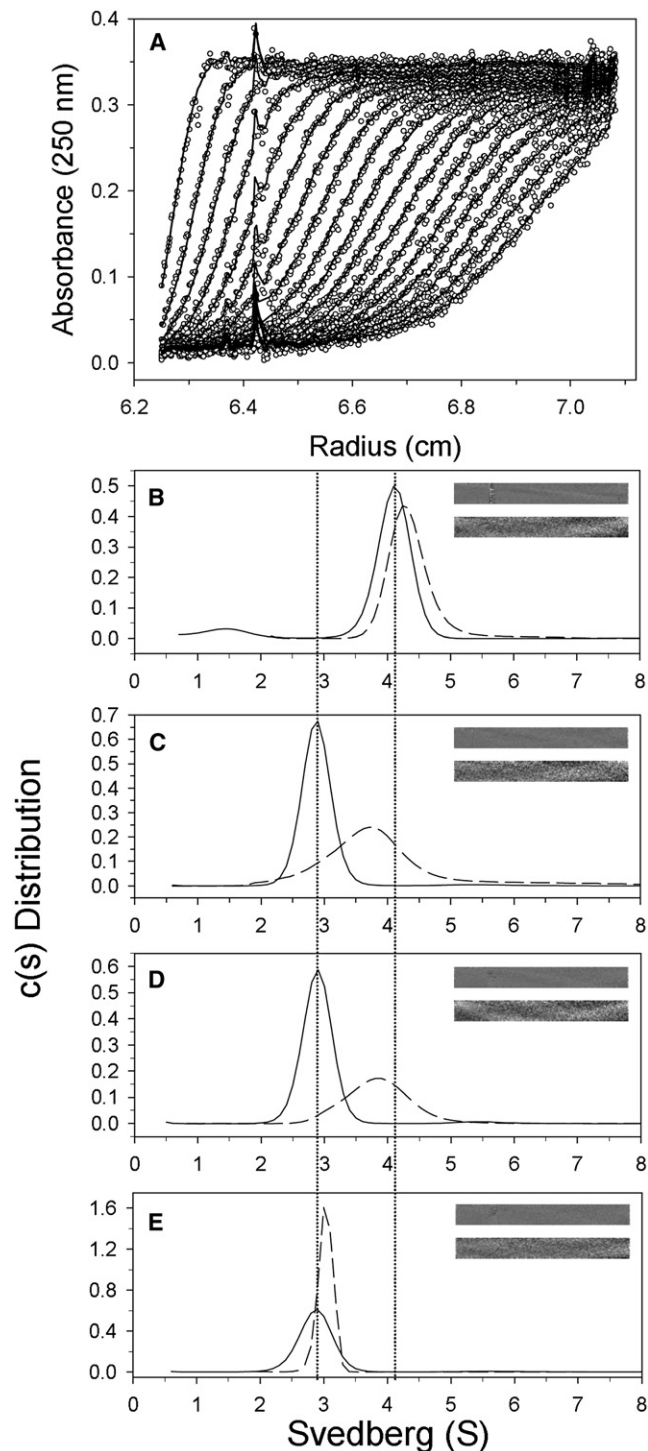


FIGURE 3 SV patterns of Mpro. (A) Typical trace of absorbance at 250 nm of the enzyme during the SV experiment. Symbols represent experimental data and lines the results fitted to the Lamm equation using the SEDFIT program (25,26). (B–E) Continuous $c(s)$ distribution of wild-type, R298A, R298L, and R298A/Q299A mutants, respectively. The residual bitmaps are shown in the insets. Protein concentration was 1.0 mg/ml. The distributions in 10 mM phosphate buffer are shown by solid lines and those in 10 mM phosphate containing 600 μM TQ6-pNA substrate by dashed lines. The left vertical dotted line indicates the monomer, and the right the dimer position.

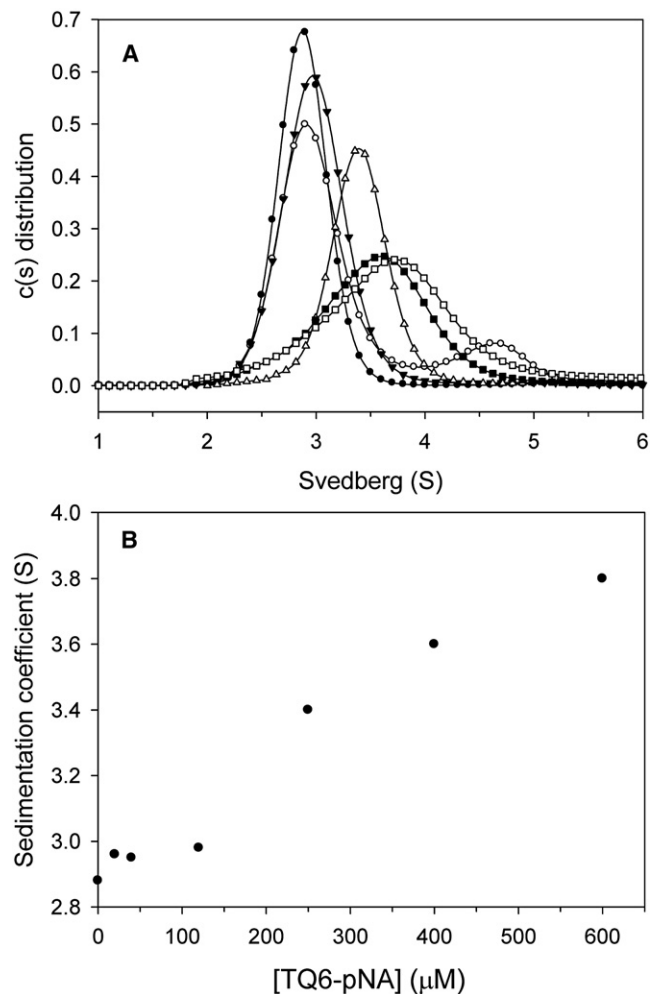


FIGURE 4 Effects of substrate concentration on the quaternary structure of the R298A mutant. (A) Continuous $c(s)$ distribution of the R298A mutant at TQ6-pNA concentrations of 0 (solid circles), 20 (open circles), 250 (open triangles), 400 (solid squares), and 600 μM (open squares). (B) Sedimentation coefficient shift of R298A major species at different TQ6-pNA concentrations.

Dimerization induced by peptide substrate is reversible

To further evaluate whether the substrate-induced dimerization is a dynamic equilibrium or a permanent, irreversible process, we performed size exclusion chromatography on Mpro and its mutants. The protease was preincubated with or without 600 μM TQ6-pNA for 20 min and then injected into the Superose 12 column (Fig. 5). The running buffer was substrate-free. The results showed that after removing the substrate, wild-type Mpro still maintained a dimeric form, but the three mutants were all monomeric. This suggests that substrate-induced dimerization is a reversible process. When the substrate leaves, the R298A/L dimers dissociate back to being a monomer. A similar result was obtained when the substrates were removed by the HiTrap desalting column (GE Healthcare, Pittsburgh, PA) and then analyzed by AUC (Fig. S3).

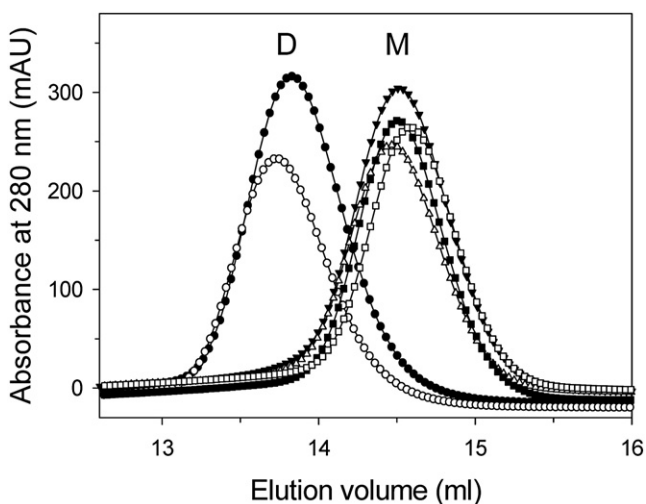


FIGURE 5 Size-exclusion chromatography of Mpro. The enzyme in phosphate-buffered saline buffer was applied to a preequilibrated Superose 12 10/300 GL column. The Mpro and its mutants, without or with preincubation in 600 μM substrate, are wild-type (solid circles), wild-type with substrate (open circles), R298A (solid triangles), R298A with substrate (open triangles), R298A/Q299A (solid squares), and R298A/Q299A with substrate (open squares).

ITC assay showed that both dimeric and monomeric Mpro can bind to the peptide substrates

Based on the structure of the SARS-CoV Mpro with its substrate analog (PDB code 1UK4), the substrate can bind by different modes to the active and inactive protomer (6). With the active protomer, the side chain of Gln-P1 accepts hydrogen bonding from the side chain of His-163 and Glu-166, resulting in specificity of Gln-P1 for the S1 subsite (Fig. 1). On the other hand, with the inactive protomer, the S1 pocket is not opened and thus does not allow the Gln-P1 to enter. Instead, Leu-P2 and Ser-P4 bind to the appropriate specific pocket. These differences imply that the substrate binding site is flexible and can undergo a significant conformational change.

To further delineate the binding of substrate to the Mpro and its mutants, we employed ITC to measure the dissociation constant (K_d for the substrate-enzyme complex), the binding enthalpy change (ΔH), and the binding stoichiometry (N) of the substrate-enzyme interaction. In the ITC experiments, 1 mM TQ6-pNA was injected into the protein solution and curve fitting based on a 1:1 binding model was carried out (Fig. 6). Compared with wild-type Mpro (Fig. 6 A), all three mutants (Fig. 6, B–D) exhibited a similar N and K_d . The N values are close to 1, which means that one substrate may bind one enzyme molecule. The K_d of substrate to wild-type Mpro was 34 μM , whereas those of substrate to R298A, R298L, and R298A/Q299A mutants were 81, 114, and 30 μM , respectively. However, the ΔH values for substrate binding to Mpro mutants were decreased by three- to sixfold compared with substrate binding to wild-

type. Although this might be an artifact, because the enzymatic hydrolysis during the titration might produce additional heat that will contribute to the overall ΔH , the ΔH , N , and K_d values from our ITC observations still suggest that the wild-type Mpro and its mutants, especially the monomeric R298A/Q299A mutant, have comparable substrate-binding affinities.

Mechanism for substrate-induced dimerization of SARS-CoV Mpro

On the basis of the solved monomeric structures (PDB codes 2QCY, 2PWX, and 3F9E), the loop of Ser-139 to Leu-141 is able to form a 3_{10} -helical structure, which results in an Asn-142 shift by 5.8 \AA (20). This shift helps the side-chain amide of Asn-142 to accept hydrogen bonding from the side chain of Glu-166 (Fig. 1). In the dimeric Mpro (PDB code 1UK3), the side chain of Glu-166 interacts with the main-chain amide of Ser-1 from protomer B (6). In the substrate-bound form (PDB code 1UK4), in protomer A, Gln-P1 enters the S1 binding pocket and its side-chain amide and carbonyl donate a hydrogen bond to the side chains of Glu-166 and His-163, respectively. Comparing these structures, the Glu-166 residue should play a distinct role. In the dimer, Glu-166 binds to the Gln-P1 of the substrate and the N-finger of protomer B. In the monomer, it shifts to interact with Asn-142, which is able to stabilize the 3_{10} -helix of Ser-139 to Leu-141.

To obtain direct evidence for the role of Glu-166, we mutated and purified E166A and E166A/R298A mutants and then performed the kinetic and quaternary structure analyses. The E166A single mutant had an ~ 3 -fold loss in enzyme activity based on k_{cat}/K_m (Table 1), whereas the enzyme activity of the E166A/R298A double mutant was not detectable. Furthermore, the experimental data from ITC for the E166A point mutant and the E166A/R298A double mutant suggest that these two mutants have comparable substrate binding affinities (Fig. S4). This indicates that without Glu-166, the substrate can still bind to the active site. On the other hand, the SV experiments suggest that E166A is a dimer with or without substrates (Fig. 7 A). Furthermore, the K_d of E166A was 3.7 μM and decreased to 0.4 μM in the presence of substrates, which was very close to the K_d for wild-type (Table 2). It is reasonable in that Glu-166 (A) \cdots Ser-1 (B) is not the main force stabilizing the dimer interface. However, when Glu-166 and Arg-298 were both mutated, the dimerization was not detected, and the K_d did not decrease in the presence of substrates (Fig. 7 B and Table 2). The results suggest that mutation of Glu-166 in R298A mutant will block the substrate-induced dimerization. This demonstrates that Glu-166 plays a pivotal role in connecting the substrate binding site with the dimer interface. The highly conserved Glu-166 in most CoVs, including SARS CoV, MHV, TGEV, HCoV, and IBV (8), implies that involvement of this residue in the protomeric communication may be universal in all virion Mpro.

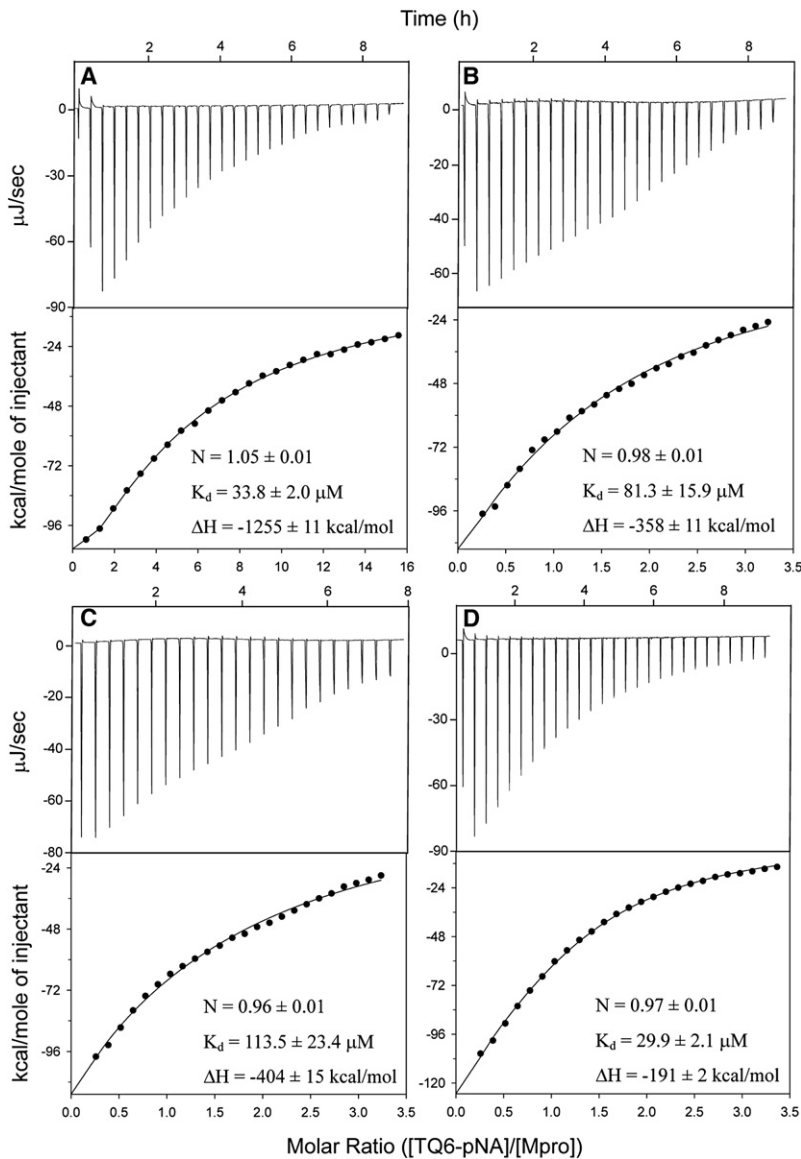


FIGURE 6 Isothermal calorimetric titration for the substrate TQ6-pNA binding to Mpro and its mutants. (A–D) Binding of TQ6-pNA to wild-type, R298A, R298L, and R298A/Q299A mutants, respectively. Wild-type protein concentration was $5.7 \mu\text{M}$ and protein concentration of the mutants was $28.6 \mu\text{M}$. The TQ6-pNA (1 mM) was titrated into 2.7 ml of protein solution using 25–30 injections at a rate of $10 \mu\text{l/injection}$. Values for the N , K_d , and ΔH were determined by ligand binding analysis with the Digitam program (TA instruments). The solid circles show the observed values and the lines represent fitted results.

To summarize the above observations, a schematic diagram showing the proposed catalytic process of SARS-CoV Mpro is presented in Fig. 8. The wild-type is a dimer, as shown in our AUC studies, but we are not very sure about the quaternary structure of Mpro under the highly diluted assay conditions ($<1.4 \mu\text{M}$). We assume that there is a rapid equilibrium between the monomer and dimer in solution. Mutation at Arg-298 will push the equilibrium to monomer. There is also a rapid equilibrium between the active and inactive protomers. Substrate binding to the protomer (either a monomer or a dimer) induces a conformational change of the enzyme that shifts the equilibrium from monomers to the catalytic-competent dimers. The protein-concentration-dependent enzyme activity experiment indicated that only the dimer is enzymatically active. Arg-298 and Gln-299 are involved in this rate-limiting step for Mpro catalysis. When both residues are mutated, there will be no substrate-

induced dimerization. On the other hand, Glu-166 is critical in the following subunit association step, which pushes the equilibrium to the catalytic-competent dimer formation. Then catalysis and release of products, followed by dissociation and regeneration of the inactive protomer, complete the catalytic cycle. This mechanism is also compatible with many current and previous studies (18,21,33,34).

CONCLUSION

In this study, we have delineated the contributions of substrate binding to Mpro dimerization. Enzyme kinetic assays indicated a nonlinear upward dependence between the enzyme activity and enzyme concentration for wild-type and R298A/L mutants. The quaternary structure of R298A/L was also changed at different enzyme concentrations. The AUC analysis proved that in the presence of

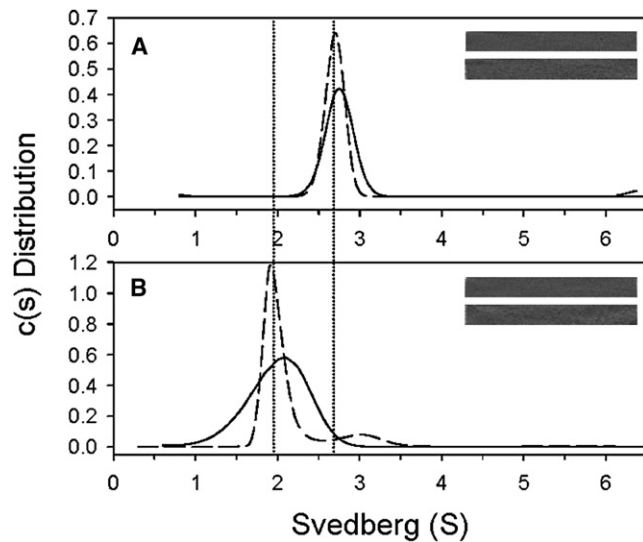


FIGURE 7 Sedimentation velocity experimental values for Glu-166 mutants E166A (A) and E166A/R298A (B) in D_2O . The protein concentration was 0.33 mg/ml. The distributions in D_2O are represented by solid lines and those in D_2O with 600 μM TQ6-pNA substrate by dashed lines. The left vertical dotted line indicates the monomer position and the right, the dimer position. (Insets) Residual bitmaps for mutants without (upper) and with (lower) substrate.

peptide substrates, the major species of the R298A/L mutants showed significant size shifting toward the dimeric form, which became clear in the D_2O environment. The substrate-induced dimerization of R298A/L was reversible upon removal of the substrates. Mutation of Glu-166 in R298A mutant significantly blocks the substrate-induced dimeriza-

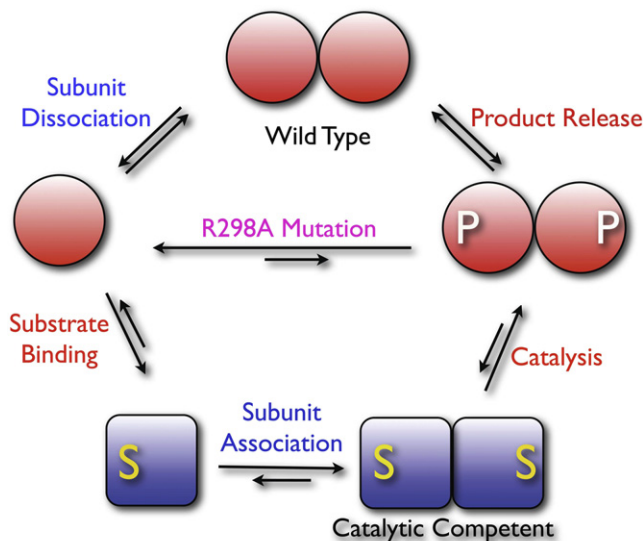


FIGURE 8 Schematic model for the catalytic process of SARS-CoV Mpro. Substrate binding triggers the monomer-dimer equilibrium to favor the active protomer (square). The active protomer now is prompt to associate, forming the catalytic-competent dimer. After the catalytic cycle, the associated dimer will dissociate again to form the inactive protomer (circle).

tion. The connection between the substrate binding site and the dimer interface by Glu-166 may be universal in all CoV Mpro. Substrate binding induces and stabilizes enzyme dimerization, which then activates the enzyme molecule.

SUPPORTING MATERIAL

Four figures are available at [http://www.biophysj.org/biophysj/supplemental/S0006-3495\(09\)06085-8](http://www.biophysj.org/biophysj/supplemental/S0006-3495(09)06085-8).

This study was supported by grants from the National Science Council, Taiwan (98-2320-B-010-026-MY3), and the National Health Research Institute, Taiwan (NHRI-EX99-9947SI), to C.Y.C. We also thank National Yang-Ming University for its financial support (Aim for Top University Plan from the Ministry of Education).

REFERENCES

1. Peiris, J. S., Y. Guan, and K. Y. Yuen. 2004. Severe acute respiratory syndrome. *Nat. Med.* 10(12, Suppl):S88–S97.
2. van der Hoek, L., K. Pyrc, ..., B. Berkhout. 2004. Identification of a new human coronavirus. *Nat. Med.* 10:368–373.
3. Woo, P. C., S. K. Lau, ..., K. Y. Yuen. 2005. Characterization and complete genome sequence of a novel coronavirus, coronavirus HKU1, from patients with pneumonia. *J. Virol.* 79:884–895.
4. Fan, K., P. Wei, ..., L. Lai. 2004. Biosynthesis, purification, and substrate specificity of severe acute respiratory syndrome coronavirus 3C-like proteinase. *J. Biol. Chem.* 279:1637–1642.
5. Hegyi, A., and J. Ziebuhr. 2002. Conservation of substrate specificities among coronavirus main proteases. *J. Gen. Virol.* 83:595–599.
6. Yang, H., M. Yang, ..., Z. Rao. 2003. The crystal structures of severe acute respiratory syndrome virus main protease and its complex with an inhibitor. *Proc. Natl. Acad. Sci. USA.* 100:13190–13195.
7. Anand, K., G. J. Palm, ..., R. Hilgenfeld. 2002. Structure of coronavirus main proteinase reveals combination of a chymotrypsin fold with an extra α -helical domain. *EMBO J.* 21:3213–3224.
8. Xue, X., H. Yu, ..., Z. Rao. 2008. Structures of two coronavirus main proteases: implications for substrate binding and antiviral drug design. *J. Virol.* 82:2515–2527.
9. Zhao, Q., S. Li, ..., Z. Rao. 2008. Structure of the main protease from a global infectious human coronavirus, HCoV-HKU1. *J. Virol.* 82:8647–8655.
10. Yang, H., W. Xie, ..., Z. Rao. 2005. Design of wide-spectrum inhibitors targeting coronavirus main proteases. *PLoS Biol.* 3:e324.
11. Bacha, U., J. Barrila, ..., E. Freire. 2008. Development of broad-spectrum halomethyl ketone inhibitors against coronavirus main protease 3CL(pro). *Chem. Biol. Drug Des.* 72:34–49.
12. Hegyi, A., A. Friebe, ..., J. Ziebuhr. 2002. Mutational analysis of the active centre of coronavirus 3C-like proteases. *J. Gen. Virol.* 83: 581–593.
13. Ziebuhr, J., S. Bayer, ..., A. E. Gorbalenya. 2003. The 3C-like proteinase of an invertebrate nidovirus links coronavirus and potyvirus homologs. *J. Virol.* 77:1415–1426.
14. Chang, H. P., C. Y. Chou, and G. G. Chang. 2007. Reversible unfolding of the severe acute respiratory syndrome coronavirus main protease in guanidinium chloride. *Biophys. J.* 92:1374–1383.
15. Zhong, N., S. Zhang, ..., B. Xia. 2009. C-terminal domain of SARS-CoV main protease can form a 3D domain-swapped dimer. *Protein Sci.* 18:839–844.
16. Chou, C. Y., H. C. Chang, ..., G. G. Chang. 2004. Quaternary structure of the severe acute respiratory syndrome (SARS) coronavirus main protease. *Biochemistry.* 43:14958–14970.

17. Hsu, W. C., H. C. Chang, ..., G. G. Chang. 2005. Critical assessment of important regions in the subunit association and catalytic action of the severe acute respiratory syndrome coronavirus main protease. *J. Biol. Chem.* 280:22741–22748.
18. Lin, P. Y., C. Y. Chou, ..., G. G. Chang. 2008. Correlation between dissociation and catalysis of SARS-CoV main protease. *Arch. Biochem. Biophys.* 472:34–42.
19. Chen, S., T. Hu, ..., X. Shen. 2008. Mutation of Gly-11 on the dimer interface results in the complete crystallographic dimer dissociation of severe acute respiratory syndrome coronavirus 3C-like protease: crystal structure with molecular dynamics simulations. *J. Biol. Chem.* 283: 554–564.
20. Hu, T., Y. Zhang, ..., X. Shen. 2009. Two adjacent mutations on the dimer interface of SARS coronavirus 3C-like protease cause different conformational changes in crystal structure. *Virology.* 388:324–334.
21. Shi, J., J. Sivaraman, and J. Song. 2008. Mechanism for controlling the dimer-monomer switch and coupling dimerization to catalysis of the severe acute respiratory syndrome coronavirus 3C-like protease. *J. Virol.* 82:4620–4629.
22. Chou, C. Y., Y. L. Lin, ..., M. S. Shiao. 2005. Structural variation in human apolipoprotein E3 and E4: secondary structure, tertiary structure, and size distribution. *Biophys. J.* 88:455–466.
23. Huang, C., P. Wei, ..., L. Lai. 2004. 3C-like proteinase from SARS coronavirus catalyzes substrate hydrolysis by a general base mechanism. *Biochemistry.* 43:4568–4574.
24. Sträter, N., L. Sun, ..., W. N. Lipscomb. 1999. A bicarbonate ion as a general base in the mechanism of peptide hydrolysis by dizinc leucine aminopeptidase. *Proc. Natl. Acad. Sci. USA.* 96:11151–11155.
25. Brown, P. H., and P. Schuck. 2006. Macromolecular size-and-shape distributions by sedimentation velocity analytical ultracentrifugation. *Biophys. J.* 90:4651–4661.
26. Schuck, P. 2000. Size-distribution analysis of macromolecules by sedimentation velocity ultracentrifugation and Lamm equation modeling. *Biophys. J.* 78:1606–1619.
27. Schuck, P. 2003. On the analysis of protein self-association by sedimentation velocity analytical ultracentrifugation. *Anal. Biochem.* 320: 104–124.
28. Shen, Y., C. Y. Chou, ..., L. Tong. 2006. Is dimerization required for the catalytic activity of bacterial biotin carboxylase? *Mol. Cell.* 22:807–818.
29. Bai, Y., T. C. Auperin, ..., L. Tong. 2007. Crystal structure of murine CstF-77: dimeric association and implications for polyadenylation of mRNA precursors. *Mol. Cell.* 25:863–875.
30. Sondermann, H., B. Nagar, ..., J. Kuriyan. 2005. Computational docking and solution x-ray scattering predict a membrane-interacting role for the histone domain of the Ras activator son of sevenless. *Proc. Natl. Acad. Sci. USA.* 102:16632–16637.
31. Barrila, J., U. Bacha, and E. Freire. 2006. Long-range cooperative interactions modulate dimerization in SARS 3CLpro. *Biochemistry.* 45:14908–14916.
32. Solowiej, J., J. A. Thomson, ..., B. W. Murray. 2008. Steady-state and pre-steady-state kinetic evaluation of severe acute respiratory syndrome coronavirus (SARS-CoV) 3CLpro cysteine protease: development of an ion-pair model for catalysis. *Biochemistry.* 47:2617–2630.
33. Chen, H., P. Wei, ..., L. Lai. 2006. Only one protomer is active in the dimer of SARS 3C-like proteinase. *J. Biol. Chem.* 281:13894–13898.
34. Hsu, M. F., C. J. Kuo, ..., P. H. Liang. 2005. Mechanism of the maturation process of SARS-CoV 3CL protease. *J. Biol. Chem.* 280: 31257–31266.
35. DeLano, W. L. 2002. The PyMOL Manual. DeLano Scientific, San Carlos, CA.